1-1-2013

Thermo-magnetic stability of superconducting films controlled by nano-morphology

V V. Yurchenko
University of Oslo

K Ilin
Karlsruhe Institute of Technology

J M. Meckbach
Karlsruhe Institute of Technology

M Siegel
Karlsruhe Institute of Technology

A J. Qviller
University of Oslo

See next page for additional authors

Thermo-magnetic stability of superconducting films controlled by nano-morphology

Abstract

Appearance of dendritic magnetic flux avalanches in superconducting films, which are associated with thermo-magnetic instability (TMI), very often indicates serious limitations for the ultimate performance of superconducting devices made of type-II superconducting thin films. We demonstrate that the stability can be controlled by a thorough adjustment of samples morphology at nano-scale, which affects internal material parameters. By this, the metal coating, commonly used as for stabilization, becomes redundant. Most importantly, we directly show by the mean of magneto-optical imaging that introduction of nano-scaled disorder dramatically changes the mode of magnetic flux propagation in the superconductors, from uniform motion of individual vortices to correlated jumps of relatively large vortex bundles, revealing the triggering mechanism of TMI. 2013 AIP Publishing LLC.

Keywords

magnetic, stability, superconducting, thermo, films, morphology, controlled, nano

Disciplines

Engineering | Physical Sciences and Mathematics

Publication Details

Yurchenko, V. V., Ilin, K., Meckbach, J. M., Siegel, M., Qviller, A. J., Galperin, Y. M. & Johansen, T. H. (2013). Thermo-magnetic stability of superconducting films controlled by nano-morphology. Applied Physics Letters, 102 (25), 252601-1-252601-5.

Authors

V V. Yurchenko, K Ilin, J M. Meckbach, M Siegel, A J. Qviller, Y M. Galperin, and Tom H. Johansen

AIP | Applied Physics Letters

Thermo-magnetic stability of superconducting films controlled by nano-morphology

V. V. Yurchenko, K. Ilin, J. M. Meckbach, M. Siegel, A. J. Qviller et al.

Citation: Appl. Phys. Lett. **102**, 252601 (2013); doi: 10.1063/1.4812484
View online: http://dx.doi.org/10.1063/1.4812484
View Table of Contents: http://apl.aip.org/resource/1/APPLAB/v102/i25
Published by the AIP Publishing LLC.

Thermo-magnetic stability of superconducting films controlled by nano-morphology

V. V. Yurchenko,[1,2,a)] K. Ilin,[3] J. M. Meckbach,[3] M. Siegel,[3] A. J. Qviller,[1] Y. M. Galperin,[1,4] and T. H. Johansen[1,5]
[1]*Department of Physics, University of Oslo, P.O. Box 1048, Blindern, 0316 Oslo, Norway*
[2]*ORG Geophysical, Tangen 10, 4070 Randaberg, Norway*
[3]*Institute of Micro- and Nanoelectronic Systems, Karlsruhe Institute of Technology, Hertzstr. 16, 76187 Karlsruhe, Germany*
[4]*A. F. Ioffe Physico-Technical Institute RAS, 194021 St. Petersburg, Russian Federation*
[5]*Institute for Superconducting and Electronic Materials, University of Wollongong, NSW 2522, Australia*

(Received 2 April 2013; accepted 12 June 2013; published online 25 June 2013)

Appearance of dendritic magnetic flux avalanches in superconducting films, which are associated with thermo-magnetic instability (TMI), very often indicates serious limitations for the ultimate performance of superconducting devices made of type-II superconducting thin films. We demonstrate that the stability can be controlled by a thorough adjustment of samples morphology at nano-scale, which affects internal material parameters. By this, the metal coating, commonly used as for stabilization, becomes redundant. Most importantly, we directly show by the mean of magneto-optical imaging that introduction of nano-scaled disorder dramatically changes the mode of magnetic flux propagation in the superconductors, from uniform motion of individual vortices to correlated jumps of relatively large vortex bundles, revealing the triggering mechanism of TMI.
 [http://dx.doi.org/10.1063/1.4812484]

External magnetic field penetrates type-II superconductors (SCs) in a quantized way in the form of Abrikosov vortices or flux lines. The Lorentz force exerted upon the vortices by shielding currents tends to set the flux lines in motion as soon as it exceeds pinning force, i.e., the interaction force between the vortices and structural irregularities of the SC. A metastable state, called the critical state[1] that corresponds to the exact balance between the two forces, can be destructed either by a magnetic flux creep or by abrupt massive flux jumps-avalanches. While the former one leads to a gradual relaxation of the flux gradient, the avalanches cause field redistribution on macro scale and may result in an immediate total loss of superconductivity due to overheating and eventual damage to a device. That takes place when the heat generated by the moving flux exceeds the heat released into environment. The phenomenon has been defined as thermo-magnetic instability (TMI) of superconductors.[2]

Besides pure academic interest, effects related to vortex dynamics in thin superconducting films are considered to be important in development of elementary base for superconducting electronics like SQUIDs,[3,4] high quality factor resonators,[5] superconducting nanowire single-photon detectors (SNSPD),[6,7] etc. SNSPD devices are currently developed for very broad spectra range from soft X-ray (both thickness d and width W of these devices are about few hundred nanometer)[8] up to infrared ($d \leq 10\,\text{nm}, W \leq 100\,\text{nm}$).[6] It has been shown that penetration and movement of magnetic vortices is one of possible mechanisms of low energy photon detection and of so called Dark Count Rate (DCR) determining a noise level of these detectors.[7,9,10] Operation of SNSPD in externally applied magnetic field was recently proposed to improve detection efficiency of these devices.[11]

One way to suppress TMI is to coat the SC with a thin layer of metal,[12,13] which provides an additional heat sink. It also hampers a rapid flux redistribution in the SC due to eddy currents induced in the normal metal.[14] However, for many applications, e.g., superconducting sensor devices, metal coating does not appear to be an acceptable option, since it is desirable to have the sensing SC uncovered. Controlling the instability via adjustment of intrinsic material parameters, provided that the key superconducting properties are not deteriorated, is therefore, of a much greater interest.

TMI exists above a certain threshold field H^{th} and below a threshold temperature T_{th}. The threshold field H^{th} is sensitive to the critical current.[15,16] In turn, the critical-current density j_c is determined by the pinning and hence, strongly linked to the material disorder. A role in development of TMI played by macro-defects, i.e., those disrupting the current flow, was recently studied in an inhomogeneous MgB_2 film.[17] Edge defects and especially cracks in such specimens tend to "concentrate" and lead magnetic flux into the sample.[18] In essence, they act as sources of strong electric field triggering the avalanches. However, reliable quantitative estimates of these fields seem to be problematic. An optimal size of the defects, which still permits analysis of experiments within the frameworks of the existing models,[2,15,19–21] lays in the range of 5–100 nm, i.e., between the coherence length ξ and penetration depth λ of SC. Such defects contribute pinning and in this way *increase* the critical current, but do not disrupt the current flow on a macroscopic scale. However, the defects *decrease* the thermal conductance,[22] facilitating the TMI. Therefore, it is hard to predict *a priori* how defects affect the stability of the critical state, and their influence requires thorough investigation.

In this work, we study TMI in a series of NbN films produced by reactive dc-magnetron sputtering of a pure Nb

a)Author to whom correspondence should be addressed. Electronic mail: vitaliy.yurchenko@fys.uio.no

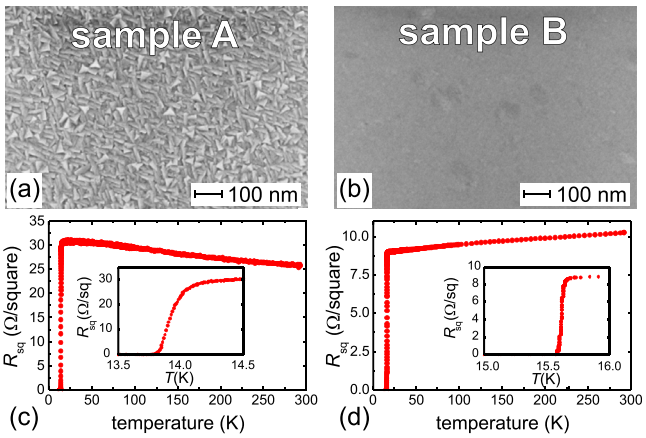

FIG. 1. SEM images of the sample surfaces are shown in (a) (sample A) and (b) (sample B) for the corresponding samples A and B. Sample A exhibits a clear nano-crystalline structure. (c) and (d) show the temperature dependence of the sheet resistances for the two samples including the enlarged transition to the superconducting state in the individual insets.

target in $Ar + N_2$ gas mixture. The NbN films with thickness $d \approx 170\,\text{nm}$ were deposited on one-side polished R-cut sapphire substrates and kept at 750 °C during the sputtering process. Two different deposition parameters were used for fabrication of samples with different nano-granularity. Since a precise determination of the granularity threshold for the appearance of TMI would require a vast amount of samples and subsequent experiments, we restrict ourselves to the two assumed limiting cases of highly granular and epitaxial films. While the sample A was deposited in a system optimized for devices that require thick layers ($d \geq 100\,\text{nm}$) at a rate of 17.7 nm/min, sample B was deposited in a system optimized for ultra-thin films ($d \leq 10\,\text{nm}$) at a rate of merely 3.6 nm/min. During patterning, particular attention was paid to the macroscopic homogeneity of the samples. In order to exclude artifacts associated with the edge roughness from further analysis, the films were patterned into a $1.5 \times 3\,\text{mm}^2$ strips using electron beam lithography and consecutive reactive ion etching, resulting in smooth edges on both samples boundaries.

Inspection of the films' surfaces by scanning electron microscopy (SEM) revealed a presence of nano-crystallites with the characteristic size of about 30 nm, Fig. 1(a) and highly uniform epitaxial structure in sample B, Fig. 1(b). The temperature dependence of the sheet resistance R_{sq} was measured by the conventional four probe method from room temperature down to 4.2 K on bridges of $\sim 1\,\mu$m in width (Figs. 1(c) and 1(d)). Sample A exhibits a $R_{sq}(300\,\text{K})/R_{sq}(25\,\text{K})$-ratio of 0.84, while sample B exhibits metallic behavior with $R_{sq}(300\,\text{K})/R_{sq}(25\,\text{K}) = 1.13$. The critical temperature T_c, determined as a temperature at which resistance of the film drops below 0.1 % of the normal state resistance R_N just above transition, was found to be 15.5 K for sample B, about 2 K higher than that of sample A. At the same time, the insets in Figs. 1(c) and 1(d) show that the width of superconducting transition, determined by 10 %/90 % criteria, is 5 times larger for the granular sample. Measurements of the second critical magnetic field B_{c2} at temperatures near T_c also demonstrate significant difference between the samples. Besides already mentioned lower T_c, sample A is characterized by almost three times steeper slope of $B_{c2}(T)$ curves. Calculated values of the electron diffusion coefficient $D = -\frac{4k_B}{\pi e} \cdot \left(\frac{dB_{c2}}{dT}\right)^{-1}$ confirm lower level of disorder of the sample B. Measured and estimated parameter of both samples are summarized in Table I for clear comparison.

For visualization of magnetic flux propagation, we exploited magneto-optical (MO) Faraday effect in Bi-substituted iron garnet films with in-plane spontaneous magnetization, grown by liquid phase epitaxy on gadolinium gallium garnet substrates. The MO indicator with a thin metallic mirror was placed on top of a SC film mounted on a cold finger in an optical helium-flow cryostat that was attached to a polarized light microscope. With polarizer and analyzer crossed 90° with respect to each other, the intensity of the image recorded with a CCD camera is proportional to a square of the local magnetic field. An external field B_{ext} was applied and controlled by a pair of resistive coils. More details of the magneto-optical setup can be found elsewhere.[21]

Magneto-optical images in Fig. 2 demonstrate the striking difference in flux dynamics in the NbN samples with and without the nano-crystallites. In the nano-granular sample A (left panel in Fig. 2), dendritic flux avalanches were observed in both ascending (Fig. 2(a)), to the upper threshold field $\mu_0 H^{th} = 71.4\,\text{mT}$, and descending fields. The flux distribution in the remanent state Fig. 2(b) demonstrates a complete collapse of the critical state in the SC. In stark contrast to its nano-granular counterpart, the epitaxial NbN film showed no signs of TMI down to $T = 3.5\,\text{K}$, the lowest temperature we could access. Results of MO imaging shown in Figs. 2(c) and 2(d) confirm the absence of TMI at $T = 4\,\text{K}$. Flux distribution in the remanent state presented in Fig. 2(d) shows no traces of the avalanches even on a descending leg of the magnetic field cycle, which is usually more susceptible to TMI.[23]

In order to explain the observed difference in the flux dynamics, we apply linear stability analysis. Several models have been developed in order to relate the SC parameters to the external criteria for the appearance and disappearance of the avalanches in bulk SC and superconducting thin films. Denisov *et al.*[20] derived an expression for the depth of the flux front ℓ^* when it becomes unstable against small fluctuations

TABLE I. Comparison of characteristic measures for sample A and sample B.

Film	d (nm)	T_c (K)	ΔT_c (K)	$-\frac{dB_{c2}}{dT}$ (T/K)	D (cm^2/s)	$\frac{R(300\,\text{K})}{R(25\,\text{K})}$	$B_{c2}(0)$ (T)	$\rho\,(25\,\text{K})$ ($\mu\Omega\,\text{cm}$)
Sample A	170	13.7	0.2	4.5	0.24	0.84	61.3	533
Sample B	175	15.5	0.04	1.7	0.64	1.13	25.6	166

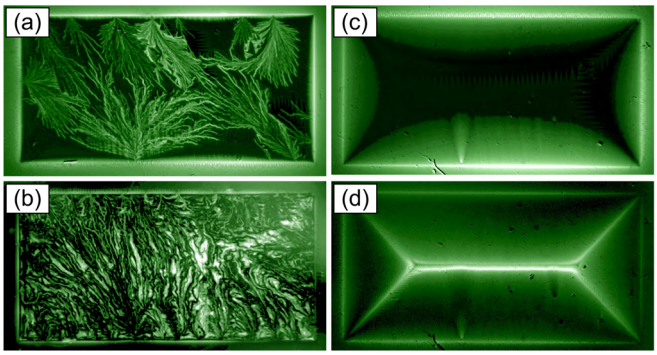

FIG. 2. Magneto-optical images of flux distribution at $T = 4\,\mathrm{K}$ in sample A (left panel) in magnetic field $\mu_0 H = 4.25$ mT (a) and in the remanent state after reaching the maximum field $\mu_0 H = 17$ mT (b); in sample B (right panel), in magnetic field $\mu_0 H = 4.25\,\mathrm{mT}$ (c) and in the remanent state after reaching the maximum field $\mu_0 H = 17\,\mathrm{mT}$ (d).

$$\ell^* = \frac{\pi}{2}\sqrt{\kappa}\left(\sqrt{\frac{j_c E}{T^*}} - \sqrt{\frac{2h_0}{nd}}\right)^{-1}, \tag{1}$$

where κ is the thermal conductivity, E is the electric field, $T^* \equiv -(\partial ln(j_c)/\partial T)^{-1}$, and h_0 is the coefficient of heat transfer from the superconducting film to the substrate. This derivation is valid for a film of thickness d where the critical current density depends on temperature and is uniform throughout the film. The parameter n characterizes the nonlinearity of the current-voltage curve of the superconductor $E \propto (j/j_c)^n$, and for NbN it is typically equal to 40. The value of applied field corresponding to onset of the TMI, H^{th}, can be obtained from ℓ^* using the Bean model relation between the penetration depth and applied field in thin films.[24] It reads as[20]

$$H^{\mathrm{th}} = \frac{j_c d}{\pi}\,\mathrm{arccosh}\left(\frac{w}{w-\ell^*}\right), \tag{2}$$

where w is half-width of the sample.

For the instability to develop, ℓ^* should be positive, finite, and smaller than w. Otherwise, when ℓ^* approaches w, the threshold field H^{th} diverges and the dendritic avalanches vanish. In turn, according to Eq. (1), ℓ^* is also divergent when the term corresponding to the heat generation, $\sqrt{j_c E/T^*}$, is outbalanced by the term corresponding to the heat release into the substrate, $\sqrt{2h_0/nd}$. Essentially the balance between the heat generation and release term serves the same purpose for SC thin films as the so-called Steckley parameter for composite superconductors, but taking into account the thermal coupling between the film and the substrate.

All the material parameters entering Eqs. (1) and (2), such as j_c, κ, T^*, and h_0, are sensitive to material disorder. We quantified the changes in these parameters imposed by the modified nano-morphology. The critical current was evaluated from MO imaging data by measuring depth of the flux front and making use of Eq. (2) in a range of temperatures between $T = 4\,\mathrm{K}$ and $T = 10\,\mathrm{K}$. At temperature $T = 4\,\mathrm{K}$, $j_{c,A}(4\mathrm{K}) = 7.75 \times 10^{10}\,\mathrm{A/m^2}$ and $j_{c,B}(4\mathrm{K}) = 2.7 \times 10^{10}\,\mathrm{A/m^2}$. The logarithmic derivative $T^* = (\partial ln(j_c)/\partial T)^{-1}$ for the two samples at $T = 4\,\mathrm{K}$ was $T^*_A \approx 0.11$ and $T^*_B = 0.16$, respectively. Changes in the thermal conductivity[25,32] become important for evaluation of the threshold field H^{th}; however, in Eq. (1), it factors out and does not change the character of the singular behavior of ℓ^*. The heat transfer into the substrate was evaluated from the hysteresis current of the (I-V) curves,[26,27] which were measured in microbridges made of satellite films, i.e., the ones deposited in the same batches with the samples: $h_{0,A}(4\,\mathrm{K}) \approx 2.49 \times 10^5\,\mathrm{Wm^{-2}K^{-1}}$ and $h_{0,B}(4\,\mathrm{K}) \approx 4.64 \times 10^5\,\mathrm{Wm^{-2}K^{-1}}$. It agrees well with the previously reported results.[28] As confirmed Stockhausen *et al.*,[27] the different measurement conditions for TMI (in vacuum) and the hysteresis current (in low pressure exchange gas) do not influence the thermal coupling of the SC strips to the environment.

Nano-defects, in the granular sample A, serve as pinning sites and provide a very homogeneous pinning landscape for the vortices, almost tripling the critical current density with respect to the smooth sample B. On the other hand, perfect morphology of the sample B, which came at a price of the reduced critical current, results in better heat conducting properties. That fits well into the qualitative understanding of the thermo-magnetic stability: the Joule heating in sample A is more intense due to the higher critical current, while the heat release is hampered by the scattering of phonons and heat-conducting normal electrons on dislocations and grain boundaries. This should promote formation of the avalanches. However, those changes alone cannot explain such a drastic difference in TMI. Given the values of the material parameters that enter Eq. (2), both samples should be stable, unless there is an enormous difference in the local electrical fields E, which as we found out was the case.

Besides the presence of the dendritic avalanches, the most important difference in the magnetic flux dynamics between the two samples was the presence of the finger-like, quasi one-dimensional (1D) micro-jumps in the sample A. Such fingers appear along all sides of the rectangular structure and their lengths scale with the depth of the flux front ℓ^*. Differential MO images presented in insets of Figs. 3(a) and 3(b) show

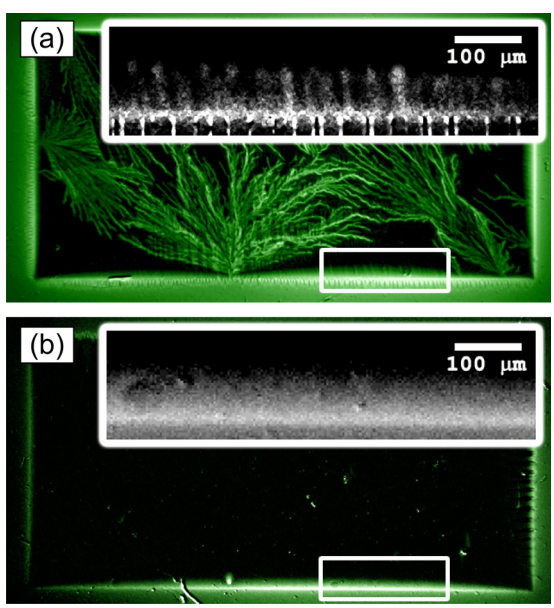

FIG. 3. Magneto-optical images of flux distribution at $T = 4\,\mathrm{K}$ in sample A (a) in magnetic field $\mu_0 H = 4.25\,\mathrm{mT}$, and sample B (b) in magnetic field $\mu_0 H = 1\,\mathrm{mT}$. Insets show differential MO images of the selected areas.

elongated bright spots in the nano-granular NbN film and virtually featureless homogeneous flux front propagation in the sample B. The images were obtained by subtracting two consecutive MO shots taken with the interval $\delta B = 42.5\,\mu$T. Each of the finger-like bright spots in the MO image of sample A corresponds to a very fast collective motion of a relatively large number of vortices, a vortex bundle, which locally induces a noticeable electric field sufficient to trigger a massive dendritic avalanche. From differential MO images, we found that the number of flux quanta in the bundles varied between few hundreds at low external fields to tens of thousands close to full penetration. For the homogeneously penetrating flux front in sample B, the electrical field can be estimated as $E(x) = \dot{B}_{\rm ext}\sqrt{(x^2 - x_{\rm p}^2)}$, where x is the coordinate in the direction of the flux propagation and $x_{\rm p}$ is the position of the flux front.[29] With the typical external field sweep rates $\dot{B}_{\rm ext} \approx 10^{-4}$–$10^{-3}\,$T/s, the electric field in sample B does not exceed $E_{\rm B} \approx 10^{-7}$–$10^{-6}\,$V/s.

In the nano-granular sample, micro-jumps occurred on a time scale shorter than an exposure time of a high speed camera, which we used in attempt to catch the jumps while they were evolving. It gave the lower estimate for the speed and the corresponding electric field due to the jumps $|E_{\rm min,A}| = |v_{\rm min} \times B_{\rm j}|$, where the local field in a jump $B_{\rm j} \approx 5\,$mT. At the external magnetic fields close to the full penetration, the length of the jumps was of the order of 0.75 mm and the characteristic time scale $\tau \sim 10^{-5}\,$s. Consequently, the lower estimates for the velocity and the electric field are $v_{\rm min} \geq 10^2\,$m/s and $E_{\rm min,A} \geq 10^{-1}\,$V/m. This remarkably high value of E coincides with the one obtained from Eq. (1) for the given set of the material parameters. With the local electric fields as high as that, the criterion for the appearance of the dendritic avalanches was apparently fulfilled.

Similar dynamic effects in quasi-1D vortex systems have been studied in $YBa_2Cu_3O_{7-\delta}$ (YBCO) films on tilted substrates.[30,31] However, unlike YBCO films, which had a well defined quasi periodic structure of planar defects, which gave rise to in-plane anisotropy of $j_{\rm c}$ and channeling of vortices, NbN films are isotropic. The origin of such an ordering in isotropic NbN samples is not yet fully understood. One possible reason for such a flux channeling may be the formation of percolative paths for vortex motion along the grain boundaries.

In conclusion, we have demonstrated a possibility to totally suppress dendritic avalanches by a thorough control of the samples nano-morphology rather than by invasive device engineering, such as introducing metal coating. Presence of the grain boundaries between the nanocrystallites promotes higher $j_{\rm c}$ by providing additional pinning sites. At the same time, diffusion of quasiparticles is noticeably hampered by the boundaries leading to the suppression of the thermal conductance and heat release into the substrate. However, the triggering of the instability is mostly governed by the dramatic difference in the mode of the flux propagation. The flux tends to move intermittently in the form of elongated quasi-1D clusters in the nano-granular sample. This gives rise to the local electric fields, leads to strong energy dissipation, and launches the positive feedback mechanism of the magnetic flux avalanches.

Fruitful and critical discussions with J. I. Vestgården, D. V. Shantsev, and J. Bergli are greatly appreciated. Magneto-optical indicators were produced by A. Solovyev and E. I. Ilyashenko. The research was in part supported by the Norwegian Research Council, project "Nano-patterned superconductors."

[1]C. Bean, Rev. Mod. Phys. **36**, 31 (1964).
[2]R. G. Mints and A. L. Rakhmanov, Rev. Mod. Phys. **53**, 551 (1981).
[3]R. C. Jaklevic, J. Lambe, A. H. Silver, and J. E. Mercereau, Phys. Rev. Lett. **12**, 159 (1964).
[4]C. D. Tesche and J. Clarke, J. Low Temp. Phys. **29**, 301 (1977).
[5]G. Hammer, S. Wuensch, M. Roesch, K. Ilin, E. Crocoll, and M. Siegel, IEEE Trans. Appl. Supercond. **19**, 565 (2009).
[6]F. Najafi, F. Marsili, E. Dauler, R. J. Molnar, and K. K. Berggren, Appl. Phys. Lett. **100**, 152602 (2012).
[7]M. Hofherr, D. Rall, K. Ilin, M. Siegel, A. Semenov, H.-W. Hubers, and N. A. Gippius, J. Appl. Phys. **108**, 014507 (2010).
[8]K. Inderbitzin, A. Engel, A. Schilling, K. Il'in, and M. Siegel, Appl. Phys. Lett. **101**, 162601 (2012).
[9]L. N. Bulaevskii, M. J. Graf, C. D. Batista, and V. G. Kogan, Phys. Rev. B **83**, 144526 (2011).
[10]H. Bartolf, A. Engel, A. Schilling, K. Il'in, M. Siegel, H.-W. Hübers, and A. Semenov, Phys. Rev. B **81**, 024502 (2010).
[11]J. R. Clem, Y. Mawatari, G. R. Berdiyorov, and F. M. Peeters, Phys. Rev. B **85**, 144511 (2012).
[12]M. Baziljevich, A. Bobyl, D. Shantsev, E. Altshuler, T. Johansen, and S. Lee, Physica C **369**, 93 (2002).
[13]E.-M. Choi, V. V. Yurchenko, T. H. Johansen, H.-S. Lee, J. Y. Lee, W. N. Kang, and S.-I. Lee, Supercond. Sci. Technol. **22**, 015011 (2009).
[14]F. Colauto, E.-M. Choi, J. Y. Lee, S. I. Lee, E. J. Patio, M. G. Blamire, T. H. Johansen, and W. A. Ortiz, Appl. Phys. Lett. **96**, 092512 (2010).
[15]V. V. Yurchenko, D. V. Shantsev, T. H. Johansen, M. R. Nevala, I. J. Maasilta, K. Senapati, and R. C. Budhani, Phys. Rev. B **76**, 092504 (2007).
[16]J. Albrecht, A. T. Matveev, J. Strempfer, H.-U. Habermeier, D. Shantsev, Y. M. Galperin, and T. H. Johansen, Phys. Rev. Lett. **98**, 117001 (2007).
[17]S. Treiber, C. Stahl, G. Schütz, and J. Albrecht, Phys. Rev. B **84**, 094533 (2011).
[18]J. I. Vestgården, D. V. Shantsev, Y. M. Galperin, and T. H. Johansen, Phys. Rev. B **76**, 174509 (2007).
[19]I. S. Aranson, A. Gurevich, M. S. Welling, R. J. Wijngaarden, V. K. Vlasko-Vlasov, V. M. Vinokur, and U. Welp, Phys. Rev. Lett. **94**, 037002 (2005).
[20]D. V. Denisov, A. L. Rakhmanov, D. V. Shantsev, Y. M. Galperin, and T. H. Johansen, Phys. Rev. B **73**, 014512 (2006); D. V. Denisov, D. V. Shantsev, Y. M. Galperin, E.-M. Choi, H.-S. Lee, S.-I. Lee, A. V. Bobyl, P. E. Goa, A. A. F. Olsen, and T. H. Johansen, Phys. Rev. Lett. **97**, 077002 (2006).
[21]V. V. Yurchenko, T. H. Johansen, and Y. M. Galperin, Low. Temp. Phys. **35**, 619 (2009).
[22]J. Bardenn, G. Rickayzen, and L. Tewordt, Phys. Rev. **113**, 982 (1959); P. M. Rowell, Proc. R. Soc. London, Ser. A **254**(1279), 542 (1960).
[23]A. Qviller, V. Yurchenko, K. Eliassen, T. Johansen, M. Nevala, I. Maasilta, K. Senapati, and R. Budhani, Physica C **470**, 897 (2010).
[24]E. H. Brandt and M. Indenbom, Phys. Rev. B **48**, 12893 (1993); E. Zeldov, J. R. Clem, M. McElfresh, and M. Darwin, *ibid.* **49**, 9802 (1994).
[25]Changes in the electronic thermal conductivity can be calculated using the expression[32] $\kappa_e = \frac{2k_{\rm B}^2 T}{\rho e^2}\left(\frac{1.76T_{\rm c}}{T}\right)^2 \exp\left(-\frac{1.76T_{\rm c}}{T}\right)$, where $k_{\rm B}$ is the Boltzmann constant, e is the electron charge, and ρ is electrical resistivity just above $T_{\rm c}$. For the two samples, $\rho_{\rm A}(25\,{\rm K}) = 533\,\mu\Omega$cm and $\rho_{\rm B}(25\,{\rm K}) = 166\,\mu\Omega$cm, and the electronic thermal conductivities are $\kappa_{\rm e,A}(4\,{\rm K}) \approx 0.002\,{\rm WK^{-2}m^{-1}}$ while $\kappa_{\rm e,B}(4\,{\rm K}) = 0.0043\,{\rm WK^{-2}m^{-1}}$.
[26]W. J. Skocpol, M. R. Beasley, and M. Tinkham, J. Appl. Phys. **45**, 4054 (1974).
[27]A. Stockhausen, K. Ilin, M. Siegel, U. Sodervall, P. Jedrasik, A. Semenov, and H.-W. Hubers, Supercond. Sci. Technol. **25**, 035012 (2012).
[28]S. Adam, L. Piraux, S. Michotte, D. Lucot, and D. Mailly, J. Phys.: Conf. Ser. **234**, 022001 (2010).
[29]E. H. Brandt, Phys. Rev. B **52**, 15442 (1995).
[30]V. Yurchenko, A. Qviller, P. Mozhaev, J. Mozhaeva, J. Hansen, C. Jacobsen, I. Kotelyanskii, A. Pan, and T. Johansen, Physica C **470**, 799 (2010).
[31]A. J. Qviller, V. V. Yurchenko, Y. M. Galperin, J. I. Vestgården, P. B. Mozhaev, J. B. Hansen, and T. H. Johansen, Phys. Rev. X **2**, 011007 (2012).
[32]A. A. Abrikosov, *Fundamentals of the Theory of Metals* (North-Holland, 1988).